

Toward engineered quantum many-body phonon systems

Ö. O. Soykal and Charles Tahan

Laboratory for Physical Sciences, 8050 Greenmead Dr, College Park, MD 20740

Arrays of coupled cavity quantum phonodynamical systems in silicon are considered. We study physical systems that can exhibit, e.g., Mott insulator states of phonons due to a strong phonon-phonon interaction (which is mediated by the impurity-cavity-phonon coupling). Our results indicate that quantum many-body phonon systems are achievable both in on-chip nanomechanical systems in silicon and DBR phonon cavity heterostructures in silicon-germanium. Experimental procedures to detect these states and temperature considerations are given. Cavity-phonon systems enable large phonon-phonon interactions while single phonons offer long wavelengths for forming extended quantum states; they may have some advantage in forming truly quantum many-body mechanical states as compared to other optomechanical systems.

PACS numbers: 64.70.Tg, 42.50.Pq, 63.20.kp, 63.22.-m

Polaritons in coupled-cavity arrays have received great interest for studying strong-correlations and collective behavior in light-matter systems [1–4]. Simultaneously, nanomechanics and optomechanics are driving toward the truly quantum regime of mechanical systems [5–9], where, for example, single photons interact with the lowest mechanical mode of a resonator. It is natural to consider whether these latter systems could exhibit many-body quantum interactions in new configurations, allowing for quantum many-body *mechanical* systems. To provide coherent and strong interaction between mechanical modes in a controlled way requires a non-linearity, however, analogous to photon blockade [10].

Optomechanical coupling—between photon and mechanical modes—may provide one avenue [8, 9] to produce quantum many-body mechanical systems. At present, however, optomechanical coupling must improve by a factor of ~ 140 to reach the quantum limit [9, 11]. Also, mechanical resonators, considered as a quantum object, have very short de Broglie wave lengths because of their mass, limiting the potential for extended quantum states. An alternate system to enable strong coupling has been proposed for acoustic phonons [12, 13], where a cavity phonon hybridizes with a semiconductor two-level system (TLS) providing a true analogue to the cavity-polariton called a cavity-phonon, which can easily enter the strong coupling regime. In addition, bulk-like single phonons in silicon can have long thermal de Broglie wave lengths, enabling extended quantum states.

In this Letter, we introduce two experimentally feasible systems where man-made many-body phonon states can be realized. We begin by identifying the physical parameter regime where many-body Jaynes-Cummings-Hubbard Hamiltonians [14–16] are realizable, finding such phases as, e.g., the Mott insulator states (“Mott lobes”). Then, as a starting point for considering real experimental setups, we consider a finite array consisting of only two cavity-TLS sites, calculating the super-splitting, the phonon blockade effect, and the response to the driving field strength which would be seen in a

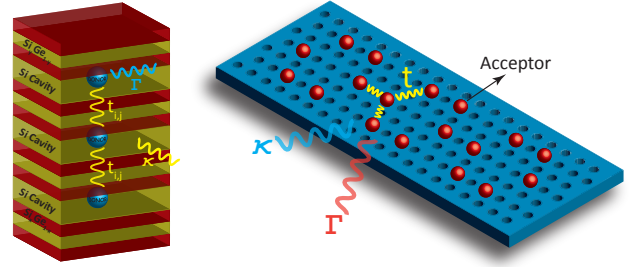


Figure 1. (color online) Schematic of a strain-matched silicon superlattice heterostructure (acoustic DBR with layers of $\text{Si}_x\text{Ge}_{1-x}/\text{Si}_y\text{Ge}_{1-y}$) containing donors is shown (left). A two-dimensional phononic crystal structure with acceptors placed at the cavity sites is also shown (right).

measurement. We conclude by considering larger system sizes, showing that extended arrays behave fundamentally differently than the small two-site model under the same hopping and driving field conditions.

Schematics of two possible realistic device designs are shown in Fig. 1. Our first device proposal involves the acoustic phonon cavities constructed from DBR heterostructures via alternating layers of $\text{Si}_x\text{Ge}_{1-x}$ [17–19]. These structures can be further engineered to possess multiple Si cavity regions in a row. In such a setup, the overall reflectivity of the layers between any two Si cavities simply relates to the phonon inter-cavity hopping frequency t_{ij} . A suitable donor placed in each of these Si cavities can be strongly coupled (a regime where coupling frequency is much larger than the donor relaxation and cavity loss rates, $g \gg \Gamma, \kappa$) to a specifically chosen single cavity-phonon mode ω , hence, forming a cavity-phonon [12]. Our second device design is directly borrowed from the concept of nano opto-mechanical phononic crystals. An engineered disturbance in periodicity can be used for trapping a desired phonon mode in a given region. Placement of an acceptor impurity into each of these regions [13] will lead to cavity-phonitons with engineered inter-cavity tunneling.

To determine the parameter range for hopping and transition frequencies of quantum phase transitions, we first consider an equilibrium system where the phonon number density is fixed. This is a good approximation where the phonon lifetime is longer than the thermalization time. For phonon arrays consisting of phosphorus donors (or boron acceptors) and phonons in a silicon phononic crystal or a DBR array (see Fig. 1), the total many-body Hamiltonian is given by the standard Jaynes-Cummings-Hubbard (JCH) model [3, 14–16, 20, 21],

$$\mathcal{H}_{JCH} = \mathcal{H}_{JC} - \sum_{\langle i,j \rangle} t_{ij} a_i^\dagger a_j, \quad (1)$$

$$\mathcal{H}_{JC} = \sum_i \left[\varepsilon \sigma_i^+ \sigma_i^- + \omega a_i^\dagger a_i + g \left(\sigma_i^+ a_i + \sigma_i^- a_i^\dagger \right) \right], \quad (2)$$

where $a_i (a_i^\dagger)$ is the phonon annihilation (creation) operator at a given cavity site i , whereas $\sigma_i^+ (\sigma_i^-)$ is the excitation (de-excitation) operator of the donor at that site. The inter-cavity phonon tunneling is given by the hopping frequency t_{ij} for the nearest neighbor cavity sites i and j . The regular Jaynes-Cummings Hamiltonian \mathcal{H}_{JC} corresponds to the interaction of a single mode of the cavity phonon with a TLS [22]. The fast oscillating terms (i.e. $\sigma_i^+ a_i^\dagger$) responsible for virtual transitions have been dropped via rotating wave approximation. The third term in Eq. (2) is solely responsible for an effective, non-linear on-site phonon repulsion in analogy with photon blockade [21, 23].

The phase transition between a Mott insulator (MI) and a superfluid phase (SF) can be determined in the grand canonical ensemble where a chemical potential μ introduced as $\mathcal{H} = \mathcal{H}_{JCH} - \mu \sum_i N_i$ fixes the number density. The operator $N = \sum_i N_i = \sum_i a_i^\dagger a_i + \sigma_i^+ \sigma_i^-$ defines the total number of excitations. For simplicity, one can assume the random on-site potential with zero mean (e.g. fluctuations of the chemical potential), $\delta\mu_i$, vanishes and t_{ij} is assumed to be a uniform short-range hopping [3, 20]. The boundary between the MI and the SF phases (Mott lobes) is determined by the value of μ for which adding or removing a particle does not require any energy. Introducing the SF order parameter, $\psi = \langle a_i \rangle$ via mean-field theory and applying the decoupling approximation, i.e. $a_i^\dagger a_j = \langle a_i^\dagger \rangle a_j + a_i^\dagger \langle a_j \rangle - \langle a_i^\dagger \rangle \langle a_j \rangle$, [14] we obtain the mean-field Hamiltonian,

$$\mathcal{H}_{MF} = \mathcal{H}_{JC} - \sum_i \left\{ z t \psi \left(a_i^\dagger + a_i \right) + z t |\psi|^2 - \mu N_i \right\}. \quad (3)$$

The correlation number z is the number of nearest neighbors in a given array geometry. Minimization of the ground state energy E of the mean-field Hamiltonian for different parameter ranges of μ , ω , and t for phosphorus (donor) and boron (acceptor) in silicon yields the Mott lobes in Fig. 2a-b. For the calculation of Mott lobes, in

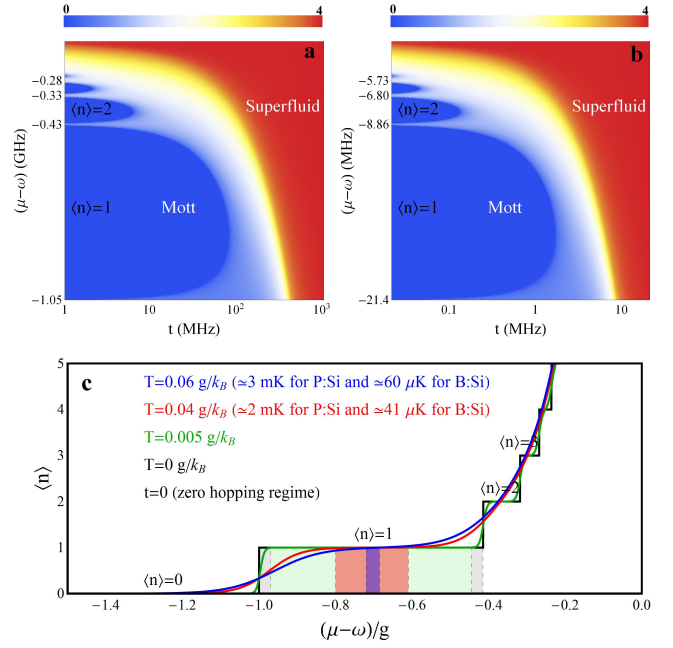


Figure 2. (color online) (a-b) For a many-body phonon-qubit system involving P:Si donors (left) and B:Si acceptors (right), the SF order parameter, ψ , is shown as a function of the phonon hopping frequency t and chemical potential μ with cavity frequency of ω . MI lobes corresponds to the regions of $\psi = 0$ (blue) where number of phonons in each lobe is constant ($\langle n \rangle = 0, 1, 2, \dots$). SF phase corresponds to $\psi \neq 0$. (c) Thermal average phonon number per site is shown for various temperatures at zero hopping. Plateaus of constant $\langle n \rangle$ corresponds to MI states.

the case of phosphorus donor impurity, acoustic DBR design with correlation number $z = 2$ (Fig. 1) is used. The donor valley states $1s(A_1)$ and $1s(T_2)$ make up the two-level system with transition frequency of $\varepsilon = 0.7$ THz corresponding to a wavelength of roughly $\lambda \approx 12$ nm [12]. Due to this small wavelength, DBR heterostructures capable of small cavity lengths are the most suitable device structures for maximal coupling. Hence, the large array of silicon/DBR heterostructure phonon cavities can be designed to support a fundamental longitudinal acoustic (LA) phonon mode in resonance with the donor transition ($\omega = \varepsilon$). In the case of the boron acceptor impurity, the transverse acoustic (TA) phonon modes of the cavities are reported to yield the maximum coupling [13]. TA phonon cavity mode of $\omega = 14$ GHz ($\lambda = 390$ nm) is needed to be in resonance with the spin splitting (in the presence of a uniform magnetic field of $B = 1$ T) of the boron valence band acting as a TLS. However, at this large wavelength, DBR phonon cavities are more difficult to construct due to the critical thickness constraint [24], and 2D phononic crystal designs [6] need to be implemented. For our calculations, we used a quality factor of $Q = 10^5$ currently achievable

Parameter	Symbol	P:Si [12]	B:Si [13]
Resonance frequency	$\omega_r/2\pi$	730 GHz	14 GHz
Coupling strength	$g/2\pi$	1 GHz	21.4 MHz
Wavelength	λ	~ 12 nm	~ 390 nm
Cavity lifetime	$1/\kappa$	22 ns	1.14 μ s
TLS lifetime	$1/\Gamma$	8.2 ns	0.14 μ s
# Rabi flops	$2g/(\kappa+\Gamma)$	~ 102	~ 34

Table I. Parameters used for a cavity phonon-TLS pair consisting of a phosphorus (P) donor or a boron (B) acceptor in silicon.

by both designs. The thermal average phonon number $\langle n \rangle$ per site versus μ for various temperatures is shown in Fig. 2c. It is defined by $\langle n \rangle = 1/Z_0 \sum_{n,\pm} n e^{-E_{n,\pm}/k_B T}$ where $E_{n,\pm} = (\omega - \mu)n + (\Delta \pm \sqrt{\Delta^2 + 4g^2n})/2$ are the energy eigenvalues of \mathcal{H}_{MF} with zero hopping and $Z_0 = \text{Tr}[e^{-\mathcal{H}_{MF}/k_B T}]$ is the grand canonical partition function for the unperturbed ($t \rightarrow 0$) system. The stable MI states (compressibility, $\partial\langle n \rangle/\partial\mu = 0$) quickly shrinks with increased temperatures. The maximum temperature allowed to access the first MI state is given as $T = 0.04\text{--}0.06$ g/k_B in terms of coupling strength.

The MI and the SF states exhibit different coherence characteristics which can be accessed via coherence (correlation) function measurements [25, 26] in setups similar to modified homodyne/heterodyne or Hanbury-Brown-Twiss. Each of these techniques generally require single phonon detectors. However, even with single phonon detectors unavailable, another useful tool, a so called the phonon-to-photon translator (PPT), can be deployed to coherently convert phonons to photons, therefore allowing the optical detection techniques to be applied on the cavity phonon-TLS system if necessary [13, 27].

The many-phonon system is driven at each site by a phonon field of amplitude Ω_i and frequency ω_d . Switching to the rotating frame of the driven field yields the time-independent Hamiltonian given by

$$\begin{aligned}
\mathcal{H}_S = & \sum_i \left[\Delta \varepsilon \sigma_i^+ \sigma_i^- + \Delta \omega a_i^\dagger a_i + g \left(\sigma_i^+ a_i + \sigma_i^- a_i^\dagger \right) \right] \\
& - \sum_{\langle i,j \rangle} t_{ij} \left(a_i^\dagger a_j + a_i a_j^\dagger \right) + \sum_i \Omega_i \left(a_i^\dagger + a_i \right) \\
= & \mathcal{H}_S^0 + \mathcal{H}_S^d,
\end{aligned} \quad (4)$$

where $\Delta \varepsilon = \varepsilon - \omega_d$ ($\Delta \omega = \omega - \omega_d$) is the detuning between the driving field and the TLS (cavity). The driving field Hamiltonian is separated as \mathcal{H}_S^d . In the case of dissipation defined by the cavity loss rate (κ) and the qubit relaxation rate (Γ), the master equation for the density matrix is given by

$$\dot{\rho} = -i[\mathcal{H}_S, \rho] + \kappa \sum_i L[a_i]\rho + \Gamma \sum_i L[\sigma_i^-]\rho, \quad (5)$$

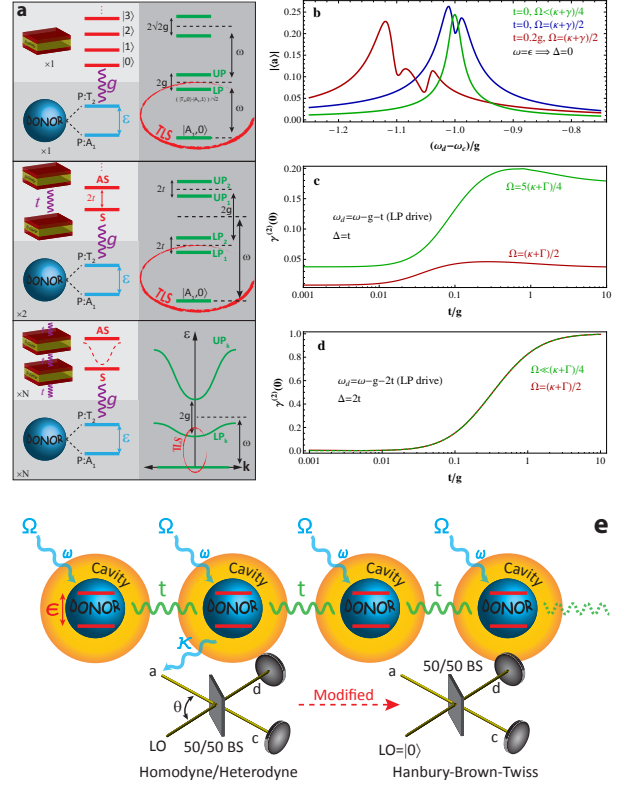


Figure 3. (color online) (a) Energy schematics of a single, two coupled, and an infinite array of coupled cavity phonon-donor pairs are shown. (b) For two coupled cavities each containing a resonant phosphorus P donor, the transmission amplitude versus the detuning between the coherent drive (ω_d) of strength $\Omega = 2\Omega_c$ and the cavity field (ω) is shown for hopping frequencies of $t = 0, t = 0.2g$. For a weak drive ($\Omega < \Omega_c$) and zero hopping $t = 0$, system exhibits a Lorentzian response (green line) (c) The second-order coherence function $\gamma^{(2)}$ versus the hopping frequency for drive strengths of $\Omega = 2\Omega_c$ and $\Omega = 5\Omega_c$, both in resonance with the LP branch ($\omega_d = \omega - g - t$). Donors are detuned by the hopping bandwidth $\Delta = t$ and in resonance with the anti-symmetric cavity-phonon mode. (d) For an infinite array, $\gamma^{(2)}$ versus hopping for $\Omega \ll \Omega_c$ and $\Omega = 2\Omega_c$. Donors detuned by $\Delta = 2t$. (e) Experimental read-out scheme from a single site by a homodyne/heterodyne or modified HBT setup.

where the Lindblad super operator is defined as $L[\hat{O}]\rho = \hat{O}\rho\hat{O}^\dagger - \{\hat{O}^\dagger\hat{O}, \rho\}/2$ [28]. The number of elements of the density matrix $\rho_{i,j}$ needs to be determined from Eq. (5) are given by $(2(\Lambda + 1))^{2n_c}$, where n_c is the number of cavities with a single donor/acceptor inside.

First, we examine the single phonon system under different driving field and hopping conditions. This can be done by driving and measuring the heterodyne amplitude of a single site in the case of zero hopping ($t = 0$) and resonance ($\varepsilon = \omega$). As seen from the Fig. 3b (green line), for weak driving field strengths smaller than the

critical value $\Omega < \Omega_c = (\kappa + \Gamma)/4$ [29], the system initially lies in the linear response regime and it exhibits a Lorentzian response to the driving field frequency. The critical coherent drive strength is estimated as $\Omega_c^P \sim 42$ MHz and $\Omega_c^B \sim 2$ MHz for a phonon composed of phosphorous donor and boron acceptor, respectively. With increasing field strengths, this response breaks down and a super-splitting [29] of the phonon field amplitude occurs (blue line). Intuitively, this behavior can be understood as a coupling of the driving field only with the antisymmetric 1st dressed state $((|0, e\rangle - |1, g\rangle)/\sqrt{2})$ and the ground state $|0, g\rangle$, therefore forming a two-level system (TLS). TLS treatment will stay valid with the driving field strength as long as the non-linearity of the Jaynes-Cummings Hamiltonian will only allow single-phonon excitations, preventing access to the higher multiple excitation manifolds, therefore, causing a phonon-blockade. In a single cavity system, the lowest two and single excitation energies are given by $\epsilon_2 = 2\omega - g\sqrt{2}$ and $\epsilon_1 = \omega - g$, respectively. This yields to the necessary condition $\Omega_i \ll g(2 - \sqrt{2})$ ($\Omega_i \ll \epsilon_2 - 2\epsilon_1$) of single excitation only subspaces of the system, also known as the "dressing of the dressed states" [30, 31]. As the single phonon system still exhibits super-splitting ($\Omega = (\kappa + \Gamma)/2$), turning on the hopping parameter ($t = 0.2g$) makes the two phonon states (one phonon in each cavity) available to occupation. This results with a clear shift in eigen frequencies and an appearance of a third peak (red line) at the heterodyne amplitude spectrum.

The second order coherence function is defined by $\gamma^{(2)}(0) = \langle a^\dagger a^\dagger a a \rangle / \langle a^\dagger a \rangle^2 = (\langle (\Delta n)^2 \rangle - \langle n \rangle^2) / \langle n \rangle^2 + 1$, where the variance is $\Delta n = n - \langle n \rangle$. MI phase is identified by $\gamma^{(2)}(0) = 1 - 1/\langle n \rangle < 1$, whereas SF phase by $\gamma^{(2)}(0) = 1$ [32]. For the two coupled phonon case, we calculated the second-order coherence function $\gamma^{(2)}$ versus the hopping frequency for different field strengths. Through out all hopping frequencies, qubits were kept detuned from their encapsulating cavity mode by $\Delta = \omega - \varepsilon = t$ to ensure a resonance with the antisymmetric mode (lowest) of the overall coupled cavity mode. At this detuning choice, the eigen energy difference between the ground state (GS) and the lower phonon (LP) branch is given by a simple relation $\Delta E = \omega - g - t$. The driving field always kept in resonance with this energy difference $\omega_d = \Delta E$ to simulate a TLS system. However, for resonant driving purposes, this detuning is not necessary, as long as one can determine the energy difference between GS and LP each time hopping and/or coupling parameters are changed. As shown in Fig. 3c, even in the case of strong driving field, $\Omega \gg \Omega_c$, the two phonon system exhibits a phonon anti-bunching.

For large cavity arrays, the mean-field theory and density matrix master equation can be applied together for weak coherent drive and strong coupling regime [25, 33]. Starting from the Hamiltonian in Eq. (4), application of the mean field $\psi = \langle a \rangle$ and decoupling approximation

yields to

$$\mathcal{H}'_{MF} = \sum_i \left[\Delta \varepsilon \sigma_i^+ \sigma_i^- + \Delta \omega a_i^\dagger a_i + g \left(\sigma_i^+ a_i + \sigma_i^- a_i^\dagger \right) - zt \left(a_i^\dagger \psi + a_i \psi^* - \psi^2 \right) + \Omega_i \left(a_i^\dagger + a_i \right) \right], \quad (6)$$

in the presence of a coherent driving field. Including the cavity loss and qubit relaxation, the master equation is same as Eq. (5) with only driven system Hamiltonian \mathcal{H}_S is replaced by the mean-field Hamiltonian \mathcal{H}'_{MF} . The SF order parameter ψ is evaluated by the self-consistency check $\psi = \text{Tr}(\rho a)$. For phonitons composed of P donors, we calculated the second-order coherence function $\gamma^{(2)}$ versus the hopping frequency for two different field strengths, $\Omega \ll \Omega_c$ and $\Omega = 2\Omega_c = 84$ MHz in Fig. 3d. For our particular donor choice, the critical drive strength is much smaller than the coupling strength $\Omega_c/g \sim 0.006$ due to already small amounts of donor relaxation and cavity loss. For a boron B acceptor, the ratio is estimated as $\Omega_c/g \sim 0.094$. The infinite phonon array exhibited a smooth transition from incoherent to coherent case, as expected, indicating a phase transition from MI to SF state by increasing the hopping frequency.

We have considered the properties of arrays of quantum phono-dynamical systems in silicon and show that small arrays will demonstrate new behavior and are realizable and measurable with present techniques. The observation of QPTs in large arrays will likely require extremely low effective temperatures (at least within the approximation considered here [34]), i.e., for P:Si, $T = 2\text{--}3$ mK ($g = 1$ GHz), and for B:Si, $T = 40\text{--}60$ μ K ($g = 21$ MHz). (Our temperature results are equally applicable to polariton arrays, making circuit-QED many-body systems equally difficult to realize.) The true nature of temperature in the phonon array system and the potential for active cooling are subjects worthy of further consideration. Our proposed many-body systems with phonons can be developed further for the pursuit of quantum simulators [35, 36] or mediators between different quantum components and potentially for new quantum devices.

We thank A. Houck, A. Mizel, and R. Ruskov for useful discussions.

Email: oneysoykal@lps.umd.edu, charlie@tahan.com

-
- [1] M. J. Hartmann, F. G. S. L. Brandao, and M. B. Plenio, *Laser & Photon. Rev.* **2**, 527 (2008).
 - [2] G. Panzarini, L. C. Adreani, A. Armitage, D. Baxter, M. S. Skolnick, V. N. Astratov, J. S. Roberts, A. V. Kavokin, M. R. Vladimirova, and M. A. Kaliteevski, *Phys. Solid State* **41**, 1223 (1999).
 - [3] J. Koch and K. L. Hur, *Phys. Rev. A* **80**, 023811 (2009).
 - [4] M. Aichhorn, M. Hohenadler, C. Tahan, and P. B. Littlewood, *Phys. Rev. Lett.* **100**, 216401 (2008).

- [5] J. D. Teufel, T. Donner, D. Li, J. W. Harlow, M. S. Allman, K. Cicak, A. J. Sirois, J. D. Whittaker, K. W. Lehnert, and R. W. Simmonds, *Nature* **475**, 359 (2011).
- [6] J. Chan, T. P. M. Alegre, A. H. Safavi-Naeini, J. T. Hill, A. Krause, S. Grblacher, M. Aspelmeyer, and O. Painter, *Nature* **478**, 89 (2011).
- [7] F. Marquardt, J. P. Chen, A. A. Clerk, and S. M. Girvin, *Phys. Rev. Lett* **99**, 093902 (2007).
- [8] S. J. M. Habraken, K. Stannigel, M. D. Lukin, P. Zoller, and P. Rabl, *New J. Phys.* **14**, 115004 (2012).
- [9] M. Ludwig, A. H. Safavi-Naeini, O. Painter, and F. Marquardt, *Phys. Rev. Lett* **109**, 063601 (2012).
- [10] P. Rabl, *Phys. Rev. Lett* **107**, 063601 (2011).
- [11] J. Chan, A. H. Safavi-Naeini, J. T. Hill, S. Meenehan, and O. Painter, *Appl. Phys. Lett* **101**, 081115 (2012).
- [12] O. O. Soykal, R. Ruskov, and C. Tahan, *Phys. Rev. Lett* **107**, 235502 (2011).
- [13] R. Ruskov and C. Tahan, arXiv:1208.1776v1 (2012).
- [14] A. D. Greentree, C. Tahan, J. H. Cole, and L. C. L. Hollenberg, *Nature Phys.* **2**, 856 (2006).
- [15] M. J. Hartmann, F. G. S. L. Brandao, and M. B. Plenio, *Nat. Phys.* **2**, 849 (2006).
- [16] M. I. Makin, J. H. Cole, C. Tahan, L. C. L. Hollenberg, and A. D. Greentree, *Phys. Rev. A* **77**, 053819 (2008).
- [17] A. J. Kent, R. N. Kini, N. M. Stanton, M. Henini, B. A. Glavin, V. A. Kochelap, and T. L. Linnik, *Phys. Rev. Lett* **96**, 215504 (2006).
- [18] Y. Ezzahri, S. Grauby, J. M. Rampnoux, H. Michel, G. Pernot, W. Claeys, and S. Dilhaire, *Phys. Rev. B* **75**, 195309 (2007).
- [19] M. Trigo, A. Bruchhausen, A. Fainstein, B. Jusserand, and V. Thierry-Mieg, *Phys. Rev. Lett* **89**, 227402 (2002).
- [20] M. P. A. Fisher, P. B. Weichman, G. Grinstein, and D. S. Fisher, *Phys. Rev. B* **40**, 546 (1989).
- [21] D. G. Angelakis, M. F. Santos, and S. Bose, *Phys. Rev. A* **76**, 031805(R) (2007).
- [22] D. Walls and G. Milburn, *Quantum Optics* (Springer-Verlag, New York, 1994).
- [23] K. M. Birnbaum, A. Boca, R. Miller, A. D. Boozer, T. E. Northup, and H. J. Kimble, *Nature* **436**, 87 (2005).
- [24] K. Brunner, *Rep. Prog. Phys* **65**, 27 (2002).
- [25] A. Tomadin, V. Giovannetti, R. Fazio, D. Gerace, I. Carusotto, H. E. Türeci, and A. Imamoglu, *Phys. Rev. A* **81**, 061801(R) (2010).
- [26] M. F. Santos, L. G. Lutterbach, S. M. Dutra, N. Zagury, and L. Davidovich, *Phys. Rev. A* **63**, 033813 (2001).
- [27] A. H. Safavi-Naeini and O. Painter, *New J. Phys.* **13**, 013017 (2011).
- [28] R. Alicki and K. Lendi, *Quantum Dynamical Semigroups and Applications* (Springer, Berlin, 2007).
- [29] L. S. Bishop, J. M. Chow, J. Koch, A. A. Houck, M. H. Devoret, E. Thuneberg, S. M. Girvin, and R. J. Schoelkopf, *Nature Phys.* **5**, 105 (2009).
- [30] S. Shamaiov, A. Parkins, M. Collett, and H. Carmichael, *Opt. Commun.* **283**, 766 (2010).
- [31] A. Nunnenkamp, J. Koch, and S. M. Girvin, *New J. Phys.* **13**, 095008 (2011).
- [32] R. J. Glauber, *Phys. Rev.* **130**, 2529 (1963).
- [33] F. Nissen, S. Schmidt, M. Biondi, G. Blatter, H. E. Türeci, and J. Keeling, *Phys. Rev. Lett.* **108**, 233603 (2012).
- [34] B. Bradlyn, F. E. A. dos Santos, and A. Pelster, *Phys. Rev. A* **79**, 013615 (2009).
- [35] R. Feynman, *Int. J. Th. Phys.* **21**, 467 (1982).
- [36] I. Buluta and F. Nori, *Science* **326**, 108 (2009).